JACS
JOURNAL OF THE AMERICAN CHEMICAL SOCIETY
Article
pubs.acs.org/JACS

An Osmium(III)/Osmium(V) Redox Couple Generating $Os^{V}(O)(OH)$ Center for *cis*-1,2-Dihydroxylation of Alkenes with H_2O_2: Os Complex with a Nitrogen-Based Tetradentate Ligand

Hideki Sugimoto,*[,†] Kazuhiro Kitayama,[†] Seiji Mori,[‡] and Shinobu Itoh*[,†]

[†]Department of Material and Life Science, Division of Advanced Science and Biotechnology, Graduate School of Engineering, Osaka University, 2-1 Yamadaoka, Suita, Osaka 565-0871, Japan

[‡]Department of Chemistry, Faculty of Science, Ibaraki University, 2-1-1 Bunkyo, Mito, Ibaraki, 310-8512, Japan

Supporting Information

ABSTRACT: For the synthesis of the 1,2-diols, *cis*-1,2-dihydroxylation of alkenes catalyzed by osmium(VIII) tetroxide (OsO_4) is a powerful method. However, OsO_4 is quite toxic due to its highly volatile and sublimable nature. Thus, the development of alternative catalysts for *cis*-1,2-dihydroxylation of alkenes is highly challenging. Our approach involves the use of a nitrogen-based tetradentate ligand, tris(2-pyridylmethyl)-amine (tpa), for an osmium center to develop a new osmium catalyst and hydrogen peroxide (H_2O_2) as a cheap and environmentally benign oxidant. The new Os–tpa complex acts as a very efficient turnover catalyst for *syn*-selective dihydroxylation of various alkenes (turnover number ~1000) in aqueous media, and H_2O_2 oxidant is formally incorporated into the products quantitatively (100% atom efficiency). The reaction intermediates involved in the catalytic cycle have been isolated and characterized crystallographically as $[Os^{III}(OH)(H_2O)(tpa)]^{2+}$ and $[Os^{V}(O)(OH)(tpa)]^{2+}$ complexes. The observed *syn*-selectivity, structural characteristics of the intermediates, and kinetic studies have suggested a concerted [3 + 2]-cycloaddition mechanism between $[Os^{V}(O)(OH)(tpa)]^{2+}$ and alkenes, which is strongly supported by DFT calculations.

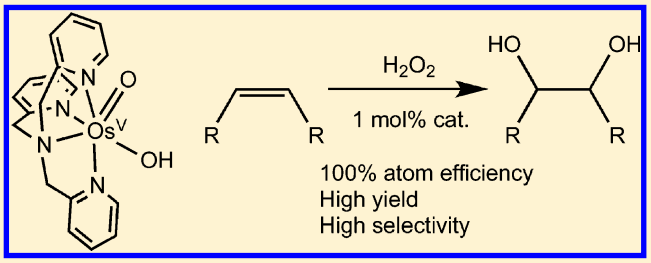

INTRODUCTION

The 1,2-diol is a common structural motif in many biologically active natural products and important synthetic intermediates of a variety of organic substances. Numerous synthetic approaches to the stereoselective *cis*-1,2-diol formation have so far been developed over the last several decades, many of which are based on direct OsO_4-catalyzed *cis*-dihydroxylation of alkenes.[1−6] Such methods are powerful and reliable, but there is a severe drawback in the use of OsO_4. The noncharged molecule OsO_4 is highly volatile and easily sublimated, and thus quite toxic (inhalation LC_{50} = 40 ppm). Especially, it causes acute poisoning to skin and eyes once it attaches to them. To avoid such risk, polymer-,[7,8] propyltrimethoxysilane-,[9] and ionic liquid[10]-supported OsO_4 have been developed and adapted to selective 1,2-dihydroxylation of a variety of alkenes.[7−10] In these cases, however, terminal oxidants are limited to NMO (*N*-methylmorpholine) or $K_3[Fe(CN)_6]$, and they should be added in a large excess.[7−10]

An alternative strategy for the catalytic *cis*-1,2-dihydroxylation of alkenes is based on the use of osmium-free complexes supported by organic ligands.[11] However, there still remain several disadvantages such as (1) substrate limitation; only electron-deficient and/or structurally constrained alkenes could be dihydroxylated;[11−13] (2) low substrate and oxidant conversion; large excess amounts of alkenes and oxidants are required;[11,12,14−16] (3) low product selectivity; significant amounts of byproducts such as epoxides and the *trans*-1,2-diols are produced;[11,12,14−16] and (4) requirements of strong oxidants such as oxone ($K[(HOO)SO_3]$)[17] and heterogeneous reagents such as acidic, neutral, and basic alumina.[18] Therefore, the efficiency of the catalytic systems so far reported is lower than that of OsO_4 itself. Moreover, mechanistic details of the reactions have yet to be clarified. On the basis of these results, osmium may still be the most desirable metal element especially for *cis*-1,2-dihydroxylation of alkenes. In this study, we tried to develop a new osmium-complex catalyst supported by a popular tetradentate ligand such as tpa [tris(2-pyridylmethyl)amine] that can collaborate with an environmentally benign and cheap oxidant H_2O_2 for selective *cis*-1,2-dihydroxylation of alkenes in aqueous media. The cationic osmium complex is neither volatile nor sublimable, and thus less toxic. The ligand may provide an octahedral osmium center having two labile coordination sites at *cis* positions. H_2O_2 is not only environmentally friendly but also provides 100% atom efficiency when it is incorporated into alkenes to give the 1,2-diols. So far, H_2O_2 was often used in the *cis*-1,2-dihydroxylation of alkenes catalyzed by OsO_4, but yields of the 1,2-diol products were lower due to nonselective product formation and overoxidations.[19−24] Even though the yields and selectivity of

Received: September 27, 2012
Published: October 30, 2012

dx.doi.org/10.1021/ja309566c | J. Am. Chem. Soc. 2012, 134, 19270−19280

the diols were improved by Bäckvall and co-workers, the protocol needs an excess amount of H_2O_2 against the substrates and NMO and flavin as the cocatalysts, making the system rather complicated.[23,24]

So far, electrochemical[25−29] and photochemical properties[30−33] of osmium-oxo coordination compounds have been investigated, but little attention has been paid to their catalytic activity. Here, we report a very efficient *cis*-1,2-dihydroxylation of alkenes with H_2O_2 in aqueous media catalyzed by a simple Os−tpa complex under very mild conditions. We have succeeded to isolate and characterize the hydroxo-aqua complex $[Os^{III}(OH)(H_2O)(tpa)](PF_6)_2$ (**2**) and the active species of oxo-hydroxo complex $[Os^{V}(O)(OH)(tpa)](ClO_4)_2$ (**3**), both of which are involved in the catalytic cycle (Chart 1).

Chart 1. ChemDraw Structures of Complexes 1, 2, and 3

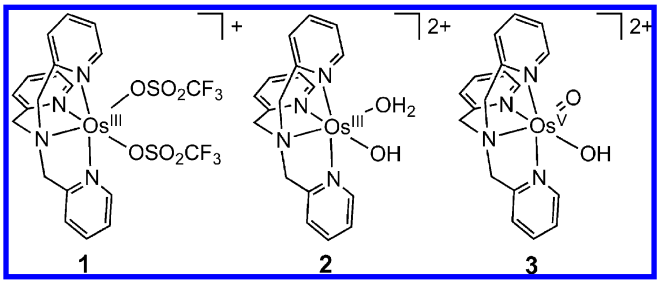

The direct reaction between isolated compound **3** and alkenes has also been investigated both kinetically and theoretically (DFT) to conclude that the reaction involves a concerted [3 + 2]-cycloaddition mechanism.

EXPERIMENTAL SECTION

Materials and Methods. *General.* The reagents and solvents used in this study except for the ligand and the complexes were commercial products of the highest available. Buffer solutions of pH 2.2, 4.0, 6.0, 8.0, and 10.0 were of *o*-$C_6H_4(COOH)(COOK)$−HCl, CH_3COOH−CH_3COONa, KH_2PO_4−Na_2HPO_4, KH_2PO_4−Na_2HPO_4, and Na_2CO_3−$NaHCO_3$, respectively, and purchased. ^1H NMR spectra were recorded at 400 MHz on a JEOL-ECP400 or a JEOL-ECS400. FT-IR spectra were recorded with a Jasco FT/IR-4100. Elemental analysis was carried out with a Yanaco CHN-Corder MT-5. ESI−mass spectra were measured with a Mariner ESI-TOF MS. Electrochemical measurements were performed with a Hokuto Denko HZ-3000. A set of carbon working electrode, SCE reference electrode, and platinum counter electrode was employed in these experiments. $[Os^{III}_2(\mu\text{-}O)(\mu\text{-}OAc)(tpa)_2](PF_6)_3$ was prepared according to the reported procedure.[34]

*$[Os^{III}(CF_3SO_3)_2(tpa)](CF_3SO_3)$ (**1**).* To $[Os^{III}_2(\mu\text{-}O)(\mu\text{-}OAc)(tpa)_2](PF_6)_3$ (100 mg, 68 μmol) in a 25 mL two-necked round bottomed flask was added fresh trifluororomethanesulfonic acid (TfOH) (1.5 mL) dropwise carefully under a dinitrogen atmosphere. The reaction mixture was stirred at 100 °C for 6 h. The flask was allowed to cool to room temperature and then cooled to ca. 5 °C in an ice bath. Diethyl ether (20 mL) was added dropwise to the stirred solution cautiously to yield microcrystalline powder, which was collected by filtration, washed with diethyl ether, and dried in vacuo. Yield: 75.7 mg (60%). Anal. Calcd for **1** ($C_{21}H_{18}N_4O_9S_3F_9Os$): C, 27.19; H, 1.96; N, 6.04. Found: C, 27.20; H, 1.97; N, 5.99. FT-IR (KBr): 1030 and 779 cm^{-1} (OTf). ESI−MS: m/z = 780 ($[M]^+$). UV−vis (acetone): λ_{max} = 420 nm (ε = 1180 M^{-1} cm^{-1}), 527 (343). CV (acetone): $E_{1/2}$ = 0.234 V vs SCE.

*$[Os^{III}(OH)(H_2O)(tpa)](PF_6)_2$ (**2**).* Complex **1** (112 mg, 121 μmol) was dissolved in water (5 mL), and the solution was heated at 70 °C for 2 h. After the solution was cooled to room temperature, 4 mL of acetate buffer solution of pH 4.0 containing an excess amount of NH_4PF_6 (200 mg, 1.23 mmol) was added to the solution. The concentration of the solution under reduced pressure to ca. 0.5 mL gave orange microcrystals. The microcrystals were collected by filtration and dried in vacuo. Yield: 74.0 mg (76%). Anal. Calcd for **2**·H_2O ($C_{18}H_{23}N_4O_3P_2F_{12}Os$): C, 26.25; H, 2.81; N, 6.80. Found: C, 26.14; H, 2.61; N, 6.68. UV−vis (H_2O): λ_{max} = 244 nm (ε = 15 200 M^{-1} cm^{-1}), 342 (6710). FT-IR (KBr): 3640 cm^{-1} (O−H), 840 (P−F). FAB-MS: m/z = 662.2 ($\{[M](PF_6)\}^+$).

*$[Os^{V}(O)(OH)(tpa)](ClO_4)_2$ (**3**).* Complex **1** (57.4 mg, 61.9 μmol) was dissolved in water (2 mL) and heated at ca. 70 °C for 2 h to generate **2** in situ. The solution was then cooled to ca. 5 °C with an ice bath, whereupon 2 equiv of cerium(IV) ammonium nitrate (71.4 mg, 133.8 μmol) dissolved in a small amount of water was added dropwise. The color of the solution immediately changed from yellow to pale sky-blue. An excess amount of $NaClO_4$ dissolved in a minimum amount of water was added to the solution, and the resultant solution was kept standing in refrigerator overnight. Sky-blue crystals precipitated from the solution, which were collected by filtration and washed with cold water, and dried in vacuo. Yield: 23.1 mg (52%). Anal. Calcd for **3**·H_2O ($C_{18}H_{21}N_4O_{11}Cl_2Os$): C, 29.59; H, 2.90; N, 7.67. Found: C, 29.47; H, 2.73; N, 7.77. FT-IR (NaCl): 881 cm^{-1} ν(Os=O), 681 and 666 ν(Os−OH). ESI−MS: m/z = 257.6 ($[M]^{2+}$). UV−vis (H_2O): λ_{max} = 253 nm (ε = 11 300 M^{-1} cm^{-1}), 290 (6140), 340 (2160), 400 (1240).

*$[Os^{V}(^{18}O)(^{18}OH)(tpa)](ClO_4)_2$ (**3***).* This complex was prepared similarly to **3** using $H_2{}^{18}O$ instead of $H_2{}^{16}O$. Yield: 50%. ESI−MS: m/z = 259.6 ($[M]^{2+}$). FT-IR (NaCl): 843 cm^{-1} ν(Os=O), 642 ν(Os−OH).

Catalytic Dihydroxylation. $[Os^{III}(CF_3SO_3)_2(tpa)](CF_3SO_3)$ (**1**) (4.65 mg, 5 μmol) in H_2O (1.5 mL) was heated to generate $[Os^{III}(OH)(OH_2)(tpa)]^{2+}$ in situ. To this solution were added *t*-BuOH (2.5 mL) and a 0.1 M acetate buffer solution (1.0 mL, pH 4.0). The combined solution was bubbled with N_2 for 30 min. The substrate (500 μmol) was then added to the solution and heated to 70 °C, and 31% H_2O_2 (49.8 μL, 500 μmol) was slowly introduced into the solution by using a syringe pump over 4 h, and the resulting mixture was allowed to stir for an additional 1 h.

Product Analysis.

(1) Dihydroxylation of cyclohexene: After the reaction, chlorobenzene (5.2 μL, 50 μmol) was added to the mixture as an internal standard. The reaction mixture was analyzed with a Shimadzu GC-14B gas chromatograph equipped with a packed column (PEG-20 M 25% Uniport B 60/80 SUS 2 m × 3 mm). The products were identified from GC retention time and ^1H NMR spectrum by comparing with those of authentic samples. The product yields were calculated from a calibration curve of a plot of mole ratio (moles of organic compound/mol of internal standard) versus area ratio (area of organic compound/area of standard).

(2) Dihydroxylation of other substrates: After the reaction, the organic products were extracted with 10 mL portions of diethyl ether five times. The combined organic layer was dried over Na_2SO_4, and after removal of Na_2SO_4 by filtration the solvent was removed by rotary evaporator. The products were identified by ^1H NMR spectrum and CI-MS by comparing those of the authentic samples. The yields of products were determined from the ^1H NMR spectra, where an integral ratio of the protons was compared to the integration ratio of the protons (Cl−C*H*− × 2) of 1,1,2,2-tetrachloroethane as an internal standard (500 μmol).

*Quantification of 1-Phenyl-1,2-ethanediol by the Reaction of $[Os^{V}(O)(OH)(tpa)](ClO_4)_2$ **3** with Styrene.* Styrene (142 mg, 1.4 mmol) was added to **3** (10 mg, 14 μmol) in an acetate buffer (pH 4.0)/*t*-BuOH mixed solvent (3.0 mL) at room temperature. The resulting solution was stirred for 3 h. The organic product was extracted with 5 mL portions of diethyl ether five times. The combined organic layer was dried over Na_2SO_4, and Na_2SO_4 was filtered off. The filtrate was removed by rotary evaporator to give a white microcrystalline powder of 1-phenyl-1,2-ethanediol in 85% yield based on **3**

dx.doi.org/10.1021/ja309566c | J. Am. Chem. Soc. 2012, 134, 19270−19280

(12 μmol). The product yield was determined from the ^{1}H NMR spectrum using 1,1,2,2-tetrachloroethane as an internal standard.

*Kinetic Measurements for the Reaction of [Os^V(O)(OH)(tpa)](ClO$_4$)$_2$ (**3**) with Styrenes.* A mixed solution of acetate buffer (pH 4.0)/*t*-BuOH (1:1, v/v) was used as the solvent throughout the experiments. The solvent was bubbled with N_2 for 30 min before the reaction. Progress of the reaction was monitored by following an increase of the absorption band at 350 nm due to $[Os^{III}(OH)(H_2O)(tpa)]^{2+}$ using an HP 5453 diode array spectrometer with a magnetic stirrer. Each reaction was initiated by adding the solution containing an excess amount of a substrate (except *p*-Cl-styrene) into the solution of **3** through the septum cap of the quartz cell (path length 1 cm) using a gastight syringe. In the case of *p*-Cl-styrene, a solution of **3** was added into the solution containing an excess amount of the substrate due to the low solubility of *p*-Cl-styrene.

X-ray Crystallography. Single crystals of **1**·$(CH_3)_2CO$ and **2**·$(CH_3)_2CO$ suitable for X-ray structural determination were obtained by slow diffusion of diethyl ether into acetone solutions of the complexes. Single crystals of **3**·H_2O were precipitated by adding $NaClO_4$ to a solution containing **2** and 2 equiv of cerium(IV) ammonium nitrate. Each single crystal of **1**·$(CH_3)_2CO$, **2**·$(CH_3)_2CO$, and **3**·H_2O was mounted on a loop with a mineral oil, and all X-ray data were collected at −165 °C on a Rigaku R-AXIS RAPID diffractmeter using filtered Mo Kα radiation. The structures were solved by direct methods (SIR 2008)[35] and expanded using Fourier techniques. The non-hydrogen atoms were refined anisotropically by full-matrix least-squares on F^2. The hydrogen atoms were attached at idealized positions on carbon atoms and were not refined. All structures in the final stages of refinement showed no movement in the atom positions. The calculations were performed using Single-Crystal Structure Analysis Software, version 3.8.[36] Crystallographic parameters are summarized in Table S1.

Computational Methodology. All calculations in the present study were performed with the Gaussian 09 program[37] and by using the unrestricted (U) Becke-three-parameter plus Lee−Yang−Parr (B3LYP) density functional theory (DFT) method.[38] The B3LYP methods were employed for Os-catalyzed hydroxylation reactions.[39−45] For all geometry optimizations and normal coordinate analyses at stationary points, we used quasi-relativistic Stuttgart−Dresden−Cologne (SDD) effective core potential and the corresponding basis set for Os,[46] and the 6-31G(d) basis set for the others. This basis set combination is termed BI in this article. Zero-point energies (ZPE) were calculated on the basis of normal coordinate analyses. Intrinsic reaction coordinate (IRC) analyses[47−49] from saddle points (transition states) to minima (reactants, intermediates, and products) were used for confirming the reaction pathways. We also employed with the larger basis set BII the SDD effective core potential[50] for Os and 6-311G(d)[51] for the others. In single point energy calculations, we used the B3LYP-D functional, which includes empirical dispersion corrections[52] and M06 functional[53] with the BII basis set. Unless noted otherwise, energies will be discussed at the B3LYP(PCM, *t*-BuOH)/BII/B3LYP/BI level. Because spin contamination in some transition states, that is, $\langle \hat{S}^2 \rangle = S(S+1)$ (S refers to total spin angular momentum), is much larger than 0.75 for doublet especially in the TSs for dihydroxylation of styrene (for example, 0.85 at the B3LYP(PCM, *t*-BuOH)/BII/B3LYP/BI level in **TSi**), we have corrected energies by removal of spin contamination, according to Yamaguchi's approximate spin projection procedure[54] in the dihydroxylation step. Details are described in the Supporting Information. Natural population analysis was performed to examine atomic charges.[55] In the single-point energy calculations, the polarizable continuum model (PCM)[56,57] with a dielectric constant of 12.5 (*t*-BuOH) was also used.[58]

RESULTS AND DISCUSSION

Catalytic *cis*-1,2-Dihydroxylation of Alkenes. Osmium(III) complex $[Os^{III}(CF_3SO_3)_2(tpa)](CF_3SO_3)$ (**1**) was synthesized by ligand substitution of μ-oxo-μ-acetato-diosmium(III) complex having tpa ligand, $[Os^{III}_2(\mu\text{-}O)(\mu\text{-}CH_3COO)(tpa)_2](PF_6)_3$,[34] with CF_3SO_3H. The weight of the isolated solid of complex **1** did not change even after standing for several weeks, indicating that **1** is neither volatile nor sublimable. Crystal structure of the complex cation is shown in Figure 1a, where the Os1 atom is coordinated with the oxygen

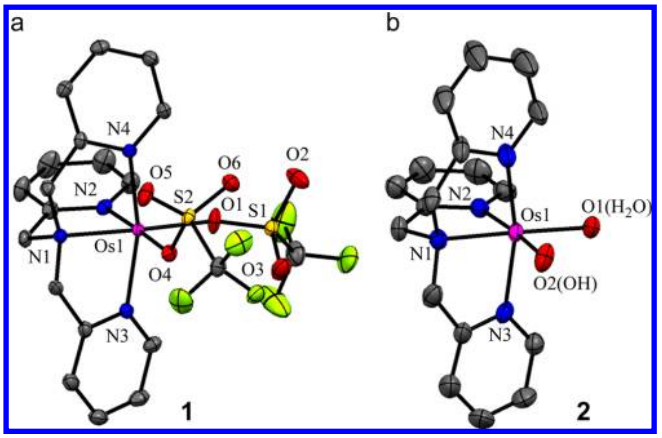

Figure 1. ORTEP drawings of (a) $[Os^{III}(CF_3SO_3)_2(tpa)](CF_3SO_3)$ (**1**) and (b) $[Os^{III}(OH)(H_2O)(tpa)](PF_6)_2$ (**2**) showing 50% probability thermal ellipsoids. The solvent molecules, hydrogen atoms, and counteranions are omitted for clarity. Selected bond lengths (Å) and angles (deg): **1**, Os1−O1 2.094(2); Os1−O4 2.099(2); Os1−N1 2.052(2); Os1−N2 2.030(2); Os1−N3 2.064(2); Os1−N4 2.073(2); O1−Os1−O4 92.23(8). **2**, Os1−O1 2.062(4); Os1−O2 2.013(5); Os1−N1 2.048(5); Os1−N2 2.056(5); Os1−N3 2.076(4); Os1−N4 2.070(5); O1−Os1−O2 91.39(17).

atoms of the two triflate anions, O1 and O4, and four nitrogen atoms of tpa ligand, N1, N2, N3, and N4. The Os1 center takes a distorted octahedral geometry as found in the dichloride derivative, $[Os^{III}Cl_2(tpa)]PF_6$,[59] and the Os1−O1 and Os1−O4 bond distances are close to each other (2.094(3) and 2.099(3) Å) despite the fact that the O1 atom is located *trans* to the tertiary amine N1, whereas the O4 atom is situated *trans* to the pyridyl nitrogen N2.

To examine the catalytic activity of the osmium complex in the alkene dihydroxylation, we first examined the reaction of cyclohexene (500 μmol) as a substrate (Table 1). An equimolar amount of H_2O_2 (500 μmol) was slowly added by using a syringe pump over 4 h to cyclohexene in a 1:1 mixed solvent system comprising *t*-BuOH (2.5 mL) and an acetate buffer solution (pH 4.0) in the presence of a catalytic amount of **1**

Table 1. Catalytic *cis*-Dihydroxylation of Cyclohexene with H_2O_2[a]

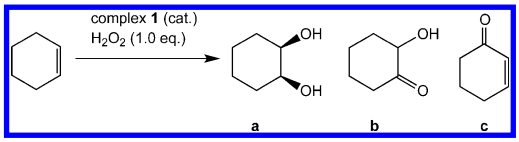

				yield (%)[b]		
entry	**1** (mol %)	temp (°C)	conv (%)	a	b	c
1	1.0	30	99	79	9	1
2	1.0	50	99	95	3	1
3	1.0	70	>99	99	1	
4	0.1	70	>99	98	2	

[a]Reaction conditions: H_2O_2 (500 μmol) and substrate (500 μmol) in acetate buffer (pH 4.0)/*t*-BuOH (2.5 mL/2.5 mL). [b]GC yield based on the substrate.

dx.doi.org/10.1021/ja309566c | J. Am. Chem. Soc. 2012, 134, 19270−19280

Table 2. Catalytic *cis*-Dihydroxylation of *n*-Octene (n = 1, 2, 3, 4)[a]

Entry	Substrate	Product	Yield (%) [b]	*Syn*-selectivity (%) [c]
1	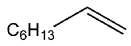	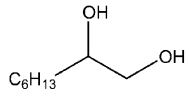	90	–
2	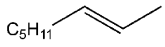	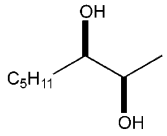 (*threo*)	83	100
3	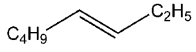	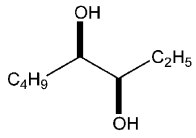 (*threo*)	57	100
4	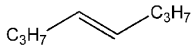	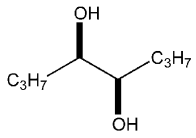 (*threo*)	55	100
5	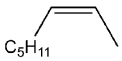	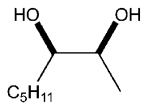 (*erythro*)	91	100
6	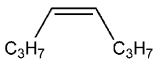	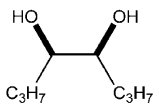 (*erythro*)	74	100

[a]Reaction conditions: **1** (1.0 mol %), H_2O_2 (500 μmol), and substrate (500 μmol) in acetate buffer (pH 4.0)/*t*-BuOH (2.5 mL/2.5 mL) at 70 °C. [b]Isolated yield. [c]Ratio of *threo*/(*threo* + *erythro*) or *erythro*/(*threo* + *erythro*).

(1.0 mol %), and the resulting solution was allowed to stir for an additional 1 h. Notably, *cis*-1,2-dihydroxylation proceeded very efficiently to give *cis*-1,2-cyclohexanediol nearly quantitatively (>99%) at 70 °C (entry 3, a trace amount of overoxidation product cyclohexanone (**b**) was obtained).[60] On the other hand, when H_2O_2 was added to the reaction solution at once, the diol yield was decreased to 62%. This may be due to a catalase type decomposition of H_2O_2 to O_2 and H_2O catalyzed by Os-complexes involved in the catalytic cycle (see below). When the reaction was carried out at lower temperature (30 and 50 °C), the yield of the diol product slightly decreased, whereas those of byproducts cyclohexanone (**b**) and 2-cyclohexene-1-one (**c**) increased (entries 1 and 2). The catalytic amount of **1** can be reduced from 1.0 to 0.1 mol % (turn over number (TON) = 980), indicating durability of the catalyst **1** (entry 4). Effects of pH of the buffer solution on the selectivity and conversion yield were also examined (pH = 2.2, 4.0, 6.0, 8.0, and 10.0, Table S2). As shown in Table S2, the dihydroxylation reaction proceeded most efficiently at weakly acidic conditions (pH 4.0, entry 2). On the other hand, under alkaline conditions (pH 10.0, entry 5), the yield of the *cis*-diol product decreased to 59% and 2-cyclohexenone was obtained in a 10% yield. Thus, the optimized reaction conditions are at 70 °C and pH 4.0. The reported *cis*-1,2-dihydroxylation of cyclohexene (1.0 mmol) with H_2O_2 (1.5 mmol) catalyzed by OsO_4 (2 mol %) proceeded in a 91% yield, but the system requires NMM (*N*-methylmorpholine, 27 mol %), flavin (5 mol %), and tetraethylammonium acetate (2 equiv).[23,24] Obviously, our system is much simpler.

Catalytic *cis*-1,2-dihydroxylation of a series of 1-, 2-, 3-, and 4-octene was then examined under the optimized reaction conditions (Table 2). In all of the cases, the corresponding 1,2-diols were obtained in high to excellent isolated yields. It is worthy to note that only the *threo* products were obtained from the *trans*-octenes, suggesting that the reaction proceeded completely via *syn*-addition (entries 2, 3, and 4). The product yield decreased in going from the terminal alkene to the internal alkenes (entries 1, 2, 3, and 4). This may be due to the

dx.doi.org/10.1021/ja309566c | J. Am. Chem. Soc. 2012, 134, 19270−19280

Table 3. Catalytic *cis*-Dihydroxylation of Various Alkenes[a]

Entry	Substrate	Product	Yield (%) [b]	*Syn*-selectivity (%) [c]
1	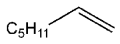	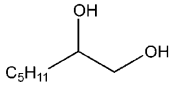	89	–
2		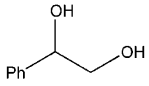	95	–
3	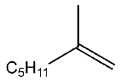	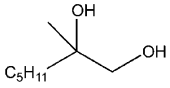	92	–
4		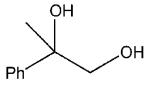	97	–
5	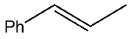	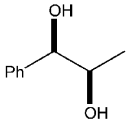 (*threo*)	92	100
6	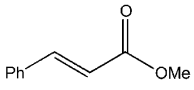	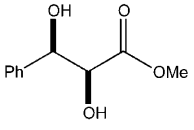 (*threo*)	89	100
7	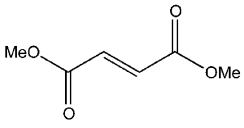	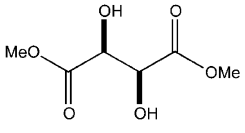 (*threo*)	65	100
8	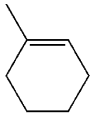	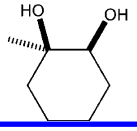	79	–

[a]Reaction conditions: **1** (1.0 mol %), H_2O_2 (500 μmol), and substrate (500 μmol) in acetate buffer (pH 4.0)/*t*-BuOH (2.5 mL/2.5 mL) at 70 °C. [b]Isolated yield. [c]Ratio of *threo*/(*threo* + *erythro*).

steric effects of the tpa ligand, because the opposite tendency was observed in the simple OsO_4/H_2O_2 system; the yield of the diol from *trans*-4-octene (34%) is higher than that from *trans*-2-octene (18%).[23] On the other hand, when *cis*-2- and *cis*-4-octenes were employed, only the *erythro* products were obtained in 91% and 74% isolated yields, respectively, where more sterically hindered *cis*-4-octene gave a lower yield. The selective formation of *erythro* products from *cis*-alkenes also confirms the *syn*-selectivity. The higher reactivity of the *cis*-alkenes when compared to the *trans*-alkenes further demonstrates that the present *cis*-dihydroxylation favors less hindered C=C double bonds.

The present catalytic reaction can be applied to *cis*-1,2-dihydroxylation of various alkenes (Table 3). The monosubstituted and 2,2-disubstituted terminal alkenes with an alkyl or a phenyl group were efficiently converted to the corresponding diols in excellent yields (entries 1–4). *syn*-Selective dihydroxylation also proceeded with alkenes having electron-withdrawing substituents in good to excellent yields (entries 5, 6, and 7). The *cis*-diol product was also obtained selectively in a good yield (79%) with a trisubstitute alkene (entry 8).

Identification of Reactive Intermediates. To elucidate the catalytic mechanism, the structure of the osmium complex formed upon dissolving $[Os^{III}(CF_3SO_3)_2(tpa)](CF_3SO_3)$ (**1**) in H_2O was investigated first. When **1** was dissolved in an acetate buffer solution (pH 4.0) at 70 °C under a dinitrogen atmosphere, a yellow solution was obtained, from which a hydroxo-aqua-osmium(III) complex $[Os^{III}(OH)(H_2O)(tpa)](PF_6)_2$ (**2**) precipitated in the presence of an excess amount of NH_4PF_6 (76% yield; the detailed procedure is given in the Experimental Section). Complex **2** exhibited the same catalytic activity as **1** in the dihydroxylation of cyclohexene, demonstrating the involvement of **2** in the catalytic cycle. The single crystals were obtained by recrystallization from acetone/diethyl ether, and the crystal structure of the cationic part of **2** is shown in Figure 1b. The Os1 atom is coordinated with the two oxygen atoms, O1 and O2, in place of the two $CF_3SO_3^-$ ligands in **1**, also adopting a distorted octahedral geometry. The Os1–O1

dx.doi.org/10.1021/ja309566c | J. Am. Chem. Soc. 2012, 134, 19270–19280

bond (2.062(4) Å) is longer than the Os1−O2 bond (2.009(4) Å), which supports the assignment of O1 atom as the aqua ligand (H_2O) and O2 atom as the hydroxo ligand (OH).

Next, the reaction of **2** with 1 equiv of H_2O_2 in an acetate buffer solution (pH 4.0) was monitored by UV−vis spectroscopy (Figure 2a). The absorption bands at 243 and 350 nm due

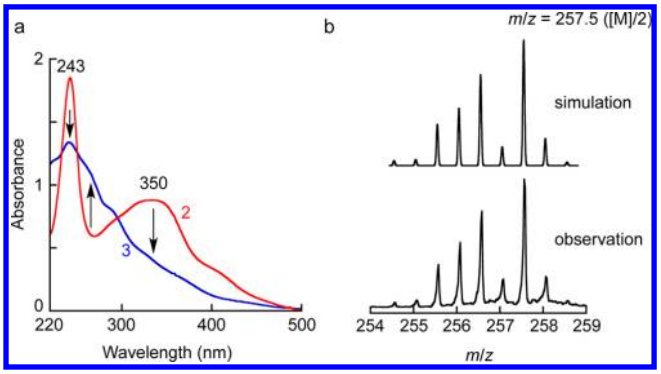

Figure 2. (a) UV−vis spectral change observed upon addition of 1 equiv of H_2O_2 to $[Os^{III}(OH)(H_2O)(tpa)]^{2+}$ (**2**) (1.0×10^{-4} M) in an acetate buffer solution (pH 4.0) (red → blue). (b) ESI−MS of the final reaction mixture of **2** and H_2O_2.

to **2** decreased with contaminant increase of new absorption bands around 250−300 nm. In the ESI−mass spectrum of the final reaction mixture, a new parent peak cluster appeared as a dicationic pattern ($[M]^{2+}$) at m/z = 257.5 (Figure 2b), which is attributable to oxo-hydroxo-osmium(V) complex, $[Os^{V}(O)(OH)(tpa)]^{2+}$ (**3**) (the spectrum in a range from m/z = 200 to 500 is given in Figure S1).[61]

Because complex **3** is formally generated by proton and electron loss from **2**, the pH-dependent cyclic voltammogram (CV) of **2** was measured in the potential range from +1.0 to −1.0 V in a 0.1 M Britton−Robbinson buffer solution. The CVs indicated that the complex can adopt oxidation states from Os(II) to Os(VI) and the redox potentials shift to a positive direction with decreasing pH of the solution. The CVs measured at pH 2.0, 4.0, 6.0, 8.0, and 10.0 are given in Figure S2 as typical examples, and Figure 3 illustrates a Pourbaix diagram ($E_{1/2}$ vs pH). When $E_{1/2}$ decreases with increasing pH with a slope of −59 and −89 mV, the redox processes involve $1H^+/1e^-$ and $3H^+/2e^-$ transfer, respectively.[62] On the other hand, when $E_{1/2}$ is independent of pH, no proton transfer is coupled with the electron transfer process.[62] From the diagram, all species generated electrochemically are identified as indicated in Figure 3. On the basis of these results, complex **3**, which is assumed to form by the reaction with H_2O_2 (see above), could be electrochemically generated in a potential range from +0.3 to +0.7 V at pH 4.0. In fact, bulk electrolysis of **2** in an acetate buffer solution (pH 4.0) at +0.60 V gave a UV−vis spectral change (Figure 4) similar to that observed in the reaction of **2** with H_2O_2 (Figure 2a). The above results clearly demonstrate that oxo-hydroxo-osmium(V) complex, **3**, was formed by the reaction of **2** with H_2O_2.[63]

Complex **3** was successfully isolated as a ClO_4^- salt, and the crystal structure was determined as shown in Figure 5. The Os1 atom has also a distorted octahedral structure with two oxygen atoms, O1 and O2, and four nitrogen atoms of tpa, N1−N4. On the basis of the shorter Os1−O1 bond (1.726(8) Å) as compared to the Os1−O2 bond (1.902(7) Å), the O1 and O2 atoms have been assigned to oxygen atoms of oxo (O) and

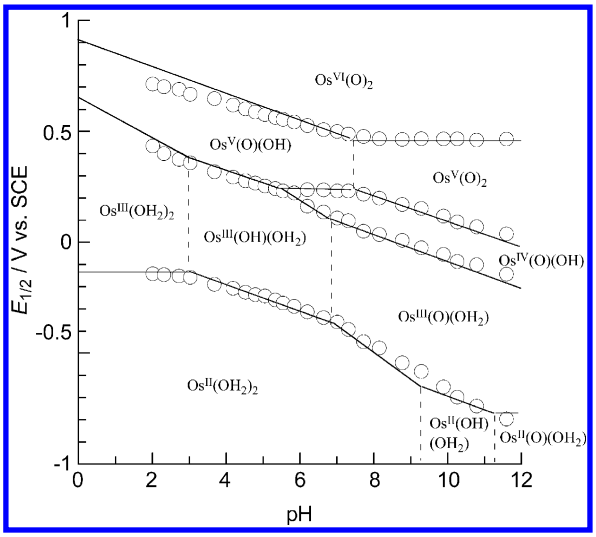

Figure 3. Pourbaix diagram for $[Os^{III}(OH)(H_2O)(tpa)]^{2+}$ (**2**). Vertical dashed lines are drawn from the breaks in the $E_{1/2}$ lines and represent approximate pK_a values.

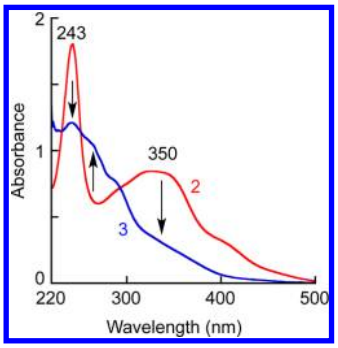

Figure 4. UV−vis spectral change observed during a bulk electrolysis of $[Os^{III}(OH)(H_2O)(tpa)]^{2+}$ (**2**) at +0.60 V vs SCE in an acetate buffer (pH 4.0). [**2**] = 1.0×10^{-4} M. Working electrode = carbon, counter electrode = Pt, reference electrode = SCE.

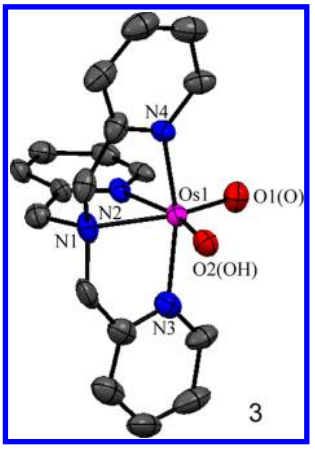

Figure 5. ORTEP drawing of $[Os^{V}(O)(OH)(tpa)](ClO_4)_2$ (**3**) showing 50% probability thermal ellipsoids. The solvent molecules, hydrogen atoms, and counteranions are omitted for clarity. Selected bond lengths (Å) and angles (deg): Os1−O1 1.726(8); Os1−O2 1.902(7); Os1−N1 2.151(7); Os1−N2 2.156(7); Os1−N3 2.070(9); Os1−N4 2.049(8); O1−Os1−O2 110.1(3).

hydroxo (OH) ligands, respectively. The O1−Os1−O2 angle became more obtuse (110.1(3)°) when compared to that of **2**

dx.doi.org/10.1021/ja309566c | J. Am. Chem. Soc. 2012, 134, 19270−19280

(91.33(17) °), due to the electronic repulsion between the two anionic oxygen atoms, O1 and O2. Next, an ^{18}O-labeled complex, $[Os^{V}(^{18}O)(^{18}OH)(tpa)](ClO_4)_2$, **3***, was synthesized by the oxidation of **2** in $H_2{}^{18}O$. In the IR spectra (Figure 6), the

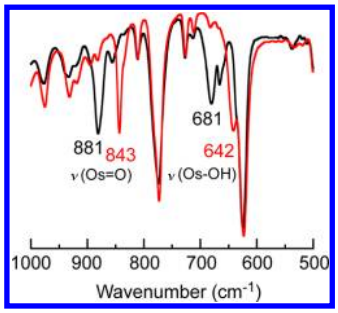

Figure 6. IR spectra of $[Os^{V}(O)(OH)(tpa)](PF_6)_2$ (**3**, black line) and ^{18}O-labeled complex (**3***, red line).

bands at 881 and 681 cm^{-1} observed for the nonlabeled complex **3** shifted to 843 and 642 cm^{-1} in the labeled **3***, respectively, (the synthetic procedure of **3*** is given in the Experimental Section). The observed ^{18}O isotopic frequency shift of −38 cm^{-1} for the former is smaller than the calculated value of −50 cm^{-1} as $\nu(Os^{V}{=}O)$ stretch from harmonic oscillator, suggesting that the band involves $\nu(Os^{V}{=}O)$ stretch coupled with other $\nu(Os^{V}{-}ligand)$ stretch. Normal coordinate analysis of **3** performed at the UB3LYP/BI level shows that **3** exhibits a vibration at 893.74 cm^{-1} corresponding to $\nu(Os^{V}{=}O)$ stretch coupled with $\nu(Os^{V}{-}N1)$ stretch. In the case of the latter shift of −39 cm^{-1} (681 to 642 cm^{-1}), the value is consistent with the calculated value as $\nu(Os^{V}{-}OH)$ stretch.

*Kinetic Analysis on Direct Reaction between **3** and Styrenes.* To get insight into the reaction mechanism of *cis*-1,2-dihydroxylation, the direct reaction of isolated oxo-hydroxo-osmium(V) compound **3** with styrene was examined. In a preparative scale reaction, **3** reacted with styrene in an acetate buffer/^{t}BuOH (1:1) solution to give the corresponding *cis*-1,2-diol in a 85% yield (the experimental procedure is given in the Experimental Section), which clearly demonstrates that **3** is the real active species of the *cis*-1,2-dihydroxylation. Next, the reaction of **3** with styrene derivatives was investigated kinetically. In Figure 7a is shown the spectral change observed upon addition of *p*-Me-styrene to an acetate buffer/*t*-BuOH (1:1, v/v) solution containing **3** (1.0×10^{-4} M) at 30 °C as a typical example, where an absorption band at 350 nm gradually

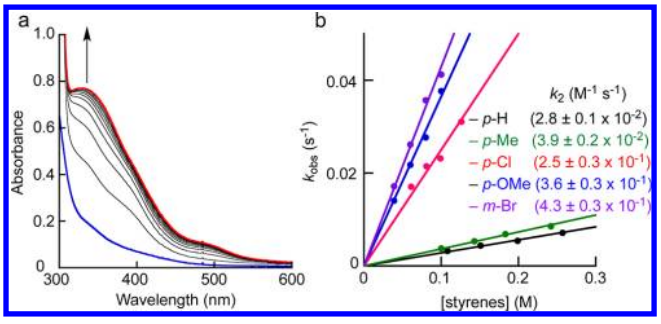

Figure 7. (a) UV−vis spectral change observed upon addition of *p*-Me-styrene (1.5×10^{-1} M) to $[Os^{V}(O)(OH)(tpa)]^{2+}$ **3** (1.0×10^{-4} M) in an acetate buffer (pH 4.0)/*t*-BuOH mixed solvent at 30 °C (100 s interval). (b) Plots of k_{obs} (observed first-order rate constants) against the substrate concentrations.

increases. The final spectrum was nearly identical to that of the hydroxo-aqua-osmium(III) complex **2**, and the corresponding diol was obtained from the final reaction mixture. The time course of the absorption change obeyed first-order kinetics, and the plot of observed first-order rate constants k_{obs} against *p*-Me-styrene concentrations gave a linear line passing through the origin, from which the second-order rate constant was determined as $k_2 = (3.9 \pm 0.2) \times 10^{-2}$ M^{-1} s^{-1} from the slope (Figure 7b). Temperature dependence on the second-order rate constant k_2 was then examined using styrene as the substrate. The plot of $\ln(k/T)$ against $1/T$ (Eyring plot) gave a straight line, from which activation parameters $\Delta H^{‡}$ and $\Delta S^{‡}$ were calculated to be +32 ± 9 kJ/mol and −169 ± 26 J/(mol K), respectively (Figures S3a and S3b). Next, electronic effects of the substituents of styrenes on the reaction rate (k_2) were investigated using various *p*- and *m*-substituted derivatives. In all of the cases, the reaction obeyed second-order kinetics, $v = k_2[\mathbf{3}][\text{styrene}]$ (Figure 7b), and the second-order rate constants thus obtained are given in Figure S4. The k_2 value increased as the substituent became more electron donating: H < *p*-Me < *p*-OMe. On the other hand, the rate constant k_2 also increased as the substituent became more electron withdrawing: H < *p*-Cl < *m*-Br. Both electron-donating and electron-withdrawing substituents of the styrenes accelerate the reaction. Similar kinetic behavior was reported in the reactions of the pseudo trigonal-bipyramidal pyridine-attached-OsO_4 complexes with styrenes.[64] In the case of the electron-rich styrenes such as *p*-MeO- and *p*-Me-styrenes, the reaction may be initiated by a nucleophilic attack of the filled π-orbital (occupied frontier MO) of the substrates to the empty π-orbital (LUMO) of **3**, whereas with electron-deficient styrenes such as *p*-Cl- and *m*-Br-styrenes, the nucleophilic attack of the filled π-orbital (HOMO) of **3** to the lowest empty π-antibonding orbitals (LUMO) of the substrates may be predominant (vide infra). Nonetheless, the largely negative $\Delta S^{‡}$ value as well as the high selectivity (*syn*-addition) strongly suggests that the reaction proceeds practically in a concerted manner as discussed below. As revealed in the crystal structure of **3**, the relatively large O1−Os1−O2 angle of **3** (110.1(3)°) is very close to the angle of regular pentagon (108°), indicating the geometry is suitable for the formation of a five-membered intermediate with alkenes via [3 + 2]-cycloaddition. Similar [3 + 2]-cycloaddition is proposed in the stoichiometric *cis*-dihydroxylation of various alkenes with $Ru^{VI}O_2$ compound, $[(Me_3tacn)(CF_3SO_2)Ru^{VI}O_2]ClO_4$ (Me_3tacn = *N*,*N*′,*N*″-1,4,7-triazacyclononane).[65] It should be also mentioned that a $Fe^{V}O(OH)$ complex supported by a similar nitrogen-based tetradentate ligand has been proposed to act as an active species in *cis*-1,2-dihydroxylation of alkenes in the model studies of iron enzyme Rieske dioxygenase.[17,66,67] The present crystallographic characterization of the $Os^{V}O(OH)$ complex **3** and its capability for selective 1,2-dihydroxylation may support the above proposal even though the catalytic efficiency of the osmium complex is much higher than that of the iron complexes.

DFT Studies and Mechanistic Consideration. To get mechanistic insight into the 1,2-dihydroxylation reaction, density functional calculations were performed. Structures of $[Os^{V}(O)(OH)(tpa)]^{2+}$ (**3**) were examined using the UB3LYP/BI method to find two conformational isomers as shown in Figure 8. In isomer **3a**, the tertiary amine atom N1 of tpa is located *trans* to the oxo group, whereas in the other isomer **3b**, the hydroxo group is situated *trans* to the N1 atom. The isomer **3a** is 18.1 kJ/mol more stable in Gibbs energy in the gas phase

dx.doi.org/10.1021/ja309566c | J. Am. Chem. Soc. 2012, 134, 19270−19280

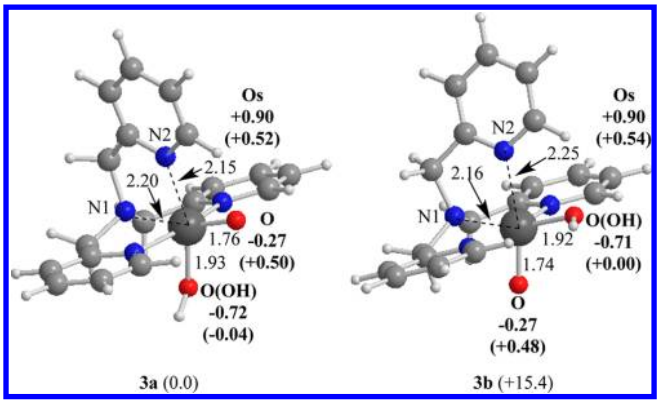

Figure 8. 3D structures of two isomers of $[Os^{V}(O)(OH)(tpa)]^{2+}$ at the B3LYP/BI level. Relative energies to the most stable isomer **3a** in kJ/mol are shown in parentheses at the B3LYP-D(PCM, *t*-BuOH)/BII//B3LYP/BI level. Atomic distances are in angstroms at the B3LYP/BI level. Natural charges and spin densities in parentheses are shown at the B3LYP/BI level.

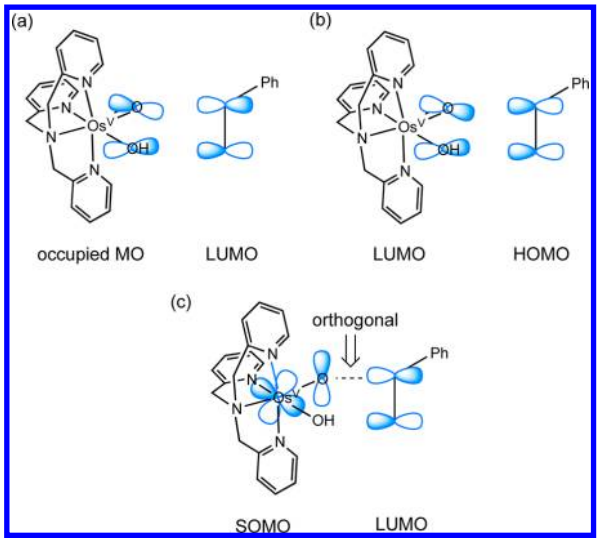

Figure 9. Representative frontier MO interactions in the [3 + 2]-type concerted transition state for the *cis*-1,2-dihydroxylation of styrene: (a) Occupied MO of **3** and LUMO of styrene, (b) LUMO of **3** and HOMO of styrene, and (c) SOMO of **3** and LUMO of styrene.

(15.4 kJ/mol more stable in electronic energy under *t*-BuOH polarity) than **3b**, consistent with the experimental result that **3** was obtained only as the **3a** isomer in the crystal (see Figure 5). Dimensions of the optimized structure of **3a** are close to those of the crystal structure; the calculated Os−O1 (oxo) bond length of 1.76 Å and the O1−Os−O2 angle of 110° are very close to those of the crystal structure of **3** (1.726(8) Å and 110.1(3)°, respectively). Natural charge of the oxo group of −0.27e is less electron negative than that of the hydroxo oxygen atom (−0.72e), while spin densities of Os and oxo group of +0.52e and +0.50e, respectively, clearly indicating a biradical character of the Os═O moiety. The SOMO of **3a** corresponds to $d\pi-p\pi$ antibonding orbital between the Os and oxo bond (see Figure S5). Some other important frontier MOs were also illustrated in Figure S5. Both αMO94 and βMO93 involve in-phase p orbital overlap of the two oxygen atoms, and αMO85 and βMO86 contain out-of-phase p orbital overlap of the two atoms. On the basis of the MO information discussed above, the schematic MO interaction between **3** and styrene is illustrated in Figure 9. The interaction between HOMO of styrene and the LUMO of **3** and the interaction between the LUMO of styrene and an occupied MO of **3** prefer a [3 + 2]-type concerted transition state (TS). Because the lobe of the C═C π^*-orbital and the SOMO of **3** is mutually orthogonal, the overlap between these orbitals may be difficult in the [3 + 2]-type TS. The [3 + 2]-type TS will be discussed in detail below.

Reaction pathways for 1,2-dihydroxylation reaction of styrene with **3** (isomer **3a**) were examined. Four transition state structures (**TSi**−**TSiv**) were obtained by geometry optimizations. Next, intrinsic reaction coordinate (IRC) analyses were carried out from the transition states downhill toward the precursor complexes (**4i**−**4iv**) and the glycolato intermediates (**5i**−**5iv**) to examine the reaction pathways. The most energetically favorable pathway through **TSi** is shown in Figure 10, and the rest is given in Figure S6. Only the most stable pathway is discussed here. The structure of a precursor complex **4i** adopts OH−π interaction between the osmium complex and the alkene moiety of styrene. **TSi** exhibits asymmetric and concerted C1··oxo and C2··OH bond formations. In **TSi**, the oxo··C1 distance of 2.04 Å is shorter than the HO··C2 distance by 0.65 Å. In the most stable **TSi**, the positive spin density of

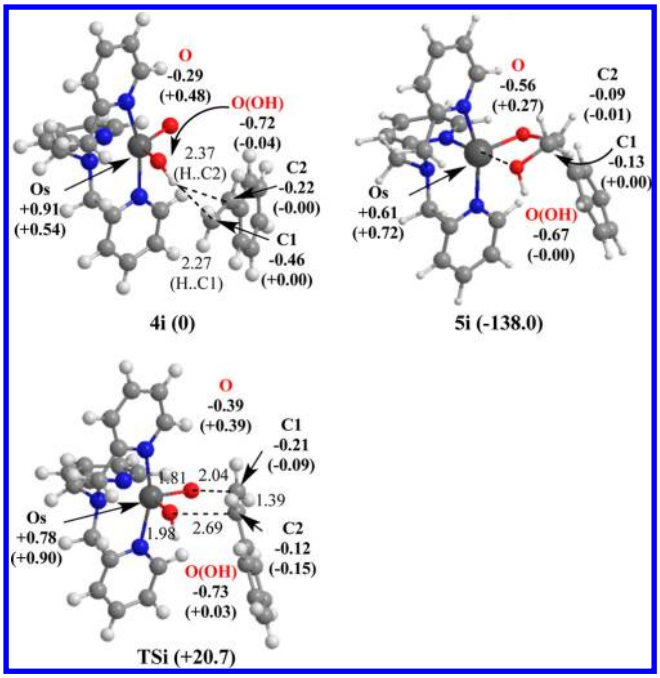

Figure 10. 3D structures of representative stationary points for the 1,2-dihydroxylation of styrene through **TSi** catalyzed by $[Os^{V}(O)(OH)(tpa)]^{2+}$ at the B3LYP/BI level. Relative energies to the precursor complex **4i** in kJ/mol are shown in parentheses at the B3LYP-D(PCM, *t*-BuOH)/BII//B3LYP/BI level. Atomic distances are in angstroms at the B3LYP/BI level. Natural charges and spin densities in parentheses are shown at the B3LYP/BI level.

the oxo group decreases from +0.48e in **4i** to +0.39e, whereas the negative spin density of the hydroxo group decreases from −0.04e in **4i** to +0.39e in **TSi**, and that of C2 increases from 0.00e in **4i** to −0.15e in **TSi**. The spin density of Os increases from +0.54e in **4i** to +0.90e in **TSi**. Finally, osmium 2-hydroxy-2-phenylethanolate **5i** was formed from **TSi**, with high exothermicity as ∼140 kJ/mol. The decrease of positive natural charge of Os in the 1,2-adduct (**5i**) of +0.61e from those in **4i** of +0.91e corresponds to the change of the oxidation number

dx.doi.org/10.1021/ja309566c | J. Am. Chem. Soc. 2012, 134, 19270−19280

Scheme 1. Proposed Reaction Mechanism for the Catalytic Dihydroxylation of Alkenes

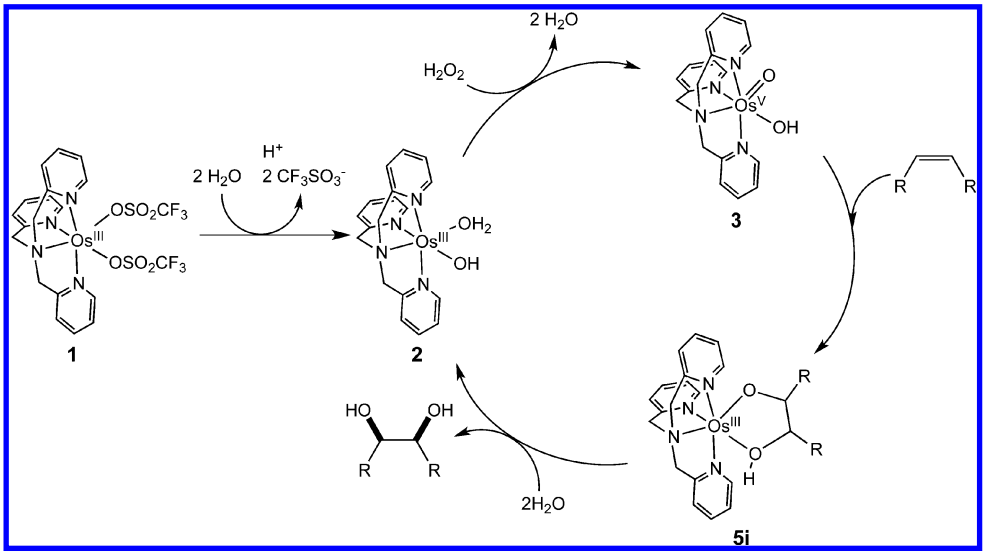

of Os from +V to +III. The spin density of the oxo group is decreased to +0.27 in **5i** as the Os−O bond is formed. The activation energy of 1,2-dihydroxylation through **TSi** at the UB3LYP-D(PCM, *t*-BuOH)/BII//B3LYP/BI level is 20.7 kJ/mol, respectively, which is compatible with the experimental activation enthalpy of +32 ± 9 kJ/mol. The Gibbs energy of activation for 1,2-dihydroxylation of dimethyl fumarate catalyzed by $Fe^{V}O(OH)(L\text{-}N_4Me_2)$ of ca. 50 kJ/mol at the B3LYP level is even higher.[17] Thus, the present theory predicts the concerted mechanism for the 1,2-dihydroxylation of styrene,[68] and the solvent polarity affects the activation energy of the Os^{V}-catalyzed 1,2-dihydroxylation of styrene.

CONCLUSION

Herein, we have demonstrated that *cis*-hydroxo-aqua-osmium(III) complex **2** supported by a tetradentate tpa ligand can catalyze selective *cis*-1,2-dihydroxylation of various alkenes using environmentally benign H_2O_2 as the oxidant in an aqueous media, where the products have been obtained in good to excellent yields based on both H_2O_2 and alkenes. Furthermore, the active species in the *cis*-1,2-dihydroxylation has been identified as *cis*-oxo-hydroxo-osmium(V) complex **3**. Both the osmium(III) and the osmium(V) complexes have been characterized by X-ray diffraction study as well as spectroscopic methods. The kinetic and theoretical studies have indicated that the *cis*-1,2-dihydroxylation involves practically a concerted [3 + 2]-cycloaddition mechanism.

A possible catalytic mechanism of the present *cis*-1,2-dihydroxylation is shown in Scheme 1. First, the ditriflate osmium(III) complex **1** is hydrolyzed to hydroxo-aqua-osmium(III) complex **2** in an acetate buffer solution (pH 4.0). Next, oxidation of **2** with 1 equiv of H_2O_2 produces the active intermediate, oxo-hydroxo-osmium(V) complex **3**, which reacts with alkene via a concerted [3 + 2]-cycloaddition mechanism to give a five-membered glycolato-osmium(III) intermediate **5i**. Finally, **5i** is hydrolyzed to give the corresponding diol product and starting complex **2**, completing the catalytic cycle. Because an osmium(III)/osmium(V) couple has not been involved in a catalytic cycle for *cis*-1,2-dihydroxylation of alkenes reported so far and the reactivity can be controlled by the supporting ligand, the present system is highly promising as an alternative method of *cis*-1,2-dihydroxylation of alkenes.

ASSOCIATED CONTENT

Supporting Information

Crystallographic data in CIF format. Further details are given in Figures S1−S6 and Tables S1−S3. Additional computational data, including coordinates and energies for all described stationary structures, and complete ref 37. This material is available free of charge via the Internet at http://pubs.acs.org.

AUTHOR INFORMATION

Corresponding Author

sugimoto@mls.eng.osaka-u.ac.jp; shinobu@mls.eng.osaka-u.ac.jp

Notes

The authors declare no competing financial interest.

ACKNOWLEDGMENTS

This work was partly supported by a grant (Grant 23350027 to H.S.) for Scientific Research (B) from the Japan Society for Promotion of Science and grants (nos. 24108725 and 24109015, Coordination Programming and Stimuli-responsive Chemical Species to H.S.) for Scientific Research on Innovative Areas from MEXT of Japan. S.I. and S.M. acknowledge financial support by a grant (nos. 22105007 and 23105507, respectively, Molecular activation) for Scientific Research on Priority Areas from MEXT of Japan. The generous allotment of computation time from the Research Center for Computational Science (RCCS), the National Institutes of Natural Sciences, Japan, is also gratefully acknowledged. We thank Mr. Kenji Ashikari for the label experiments in the catalytic dihydroxylation.

REFERENCES

(1) Kolb, H. C.; VanNieuwenhze, M. S.; Sharpless, K. B. *Chem. Rev.* **1994**, *94*, 2483−2547.

(2) Kolb, H. C.; Sharpless, K. B. In *Transition Metals for Organic Synthesis*; Beller, M., Bolm, C., Eds.; Wiley-VCH: Winheim, Germany, 2004; Vol. 2.

(3) Zaitsev, A. B.; Adolfsson, H. *Synthesis* **2006**, 1725−1756.

(4) VanRheenen, V.; Kelly, R. C.; Cha, D. F. *Tetrahedron Lett.* **1976**, *17*, 1973−1976.

(5) Jacobsen, E. N.; Markd, I.; Schrcider, G.; Sharpless, K. B. *J. Am. Chem. Soc.* **1988**, *110*, 1968−1970.
(6) Minoto, M.; Yamamoto, K.; Tsuji, J. *J. Org. Chem.* **1990**, *55*, 766−768.
(7) Kobayashi, S.; Endo, M.; Nagayama, S. *J. Am. Chem. Soc.* **1999**, *121*, 11229−11230.
(8) Kobayashi, S.; Ishida, T.; Akiyama, R. *Org. Lett.* **2001**, *3*, 2649−2652.
(9) Severeyns, A.; Vos, D. E. E.; Fiermans, L.; Verpoort, F.; Grobet, P. J.; Jacobs, P. A. *Angew. Chem., Int. Ed.* **2001**, *40*, 586−589.
(10) Yao, Q. *Org. Lett.* **2002**, *4*, 2197−2199.
(11) Bataille, C. J. R.; Donohoe, T. J. *Chem. Soc. Rev.* **2011**, *40*, 114−118.
(12) Fujita, M.; Costas, M.; Que, L., Jr. *J. Am. Chem. Soc.* **2003**, *125*, 9912−9913.
(13) De Boer, J. W.; Brinksma, J.; Browne, W. R.; Meetsma, A.; Alsters, P. L.; Hage, R.; Feringa, B. L. *J. Am. Chem. Soc.* **2005**, *127*, 7990−7991.
(14) Suzuki, K.; Oldenbug, P. D.; Que, L., Jr. *Angew. Chem., Int. Ed.* **2008**, *47*, 1887−1889.
(15) Bruijnincx, P. C. A.; Buurmans, I. L. C.; Gosiewska, S.; Moelands, M. A. H.; Lutz, M.; Spek, A. L.; Koten, G.; Gebbink, R. J. M. K. *Chem.-Eur. J.* **2008**, *14*, 1228−1237.
(16) Oldenburg, P. D.; Geng, Y.; Pryjomska-Ray, I.; Ness, D.; Que, L., Jr. *J. Am. Chem. Soc.* **2010**, *132*, 17713−17723.
(17) Chow, T. W-A.; Wong, E. L.-M.; Guo, Z.; Liu, Y.; Huang, J.-S.; Che, C.-M. *J. Am. Chem. Soc.* **2010**, *132*, 13229−13239.
(18) Yip, W.-P.; Ho, C.-M.; Zhu, N.; Lau, T.-C.; Che, C.-M. *Chem.-Asian J.* **2008**, *3*, 70−77.
(19) Milas, N. A.; Sussman, S. *J. Am. Chem. Soc.* **1936**, *58*, 1302−1304.
(20) Milas, N. A.; Sussman, S. *J. Am. Chem. Soc.* **1937**, *59*, 2345−2347.
(21) Milas, N. A.; Sussman, S.; Mason, H. S. *J. Am. Chem. Soc.* **1939**, *61*, 1844−1847.
(22) Milas, N. A.; Trepagnier, J. H.; Nolan, J. T., Jr.; Iliopulos, M. I. *J. Am. Chem. Soc.* **1959**, *81*, 4730−4733.
(23) Begstad, K.; Jonsson, S. Y.; Bäckvall, J.-E. *J. Am. Chem. Soc.* **1999**, *121*, 10424−10425.
(24) Jonsson, S. Y.; Färnegardh, K.; Bäckvall, J.-E. *J. Am. Chem. Soc.* **2001**, *123*, 1365−1371.
(25) Dobson, J. C.; Takeuchi, K. J.; Pipes, D. W.; Geselowitz, D. A.; Meyer, T. J. *Inorg. Chem.* **1986**, *25*, 2357−2365.
(26) Pipes, D. W.; Meyer, T. J. *Inorg. Chem.* **1986**, *25*, 4042−4050.
(27) Kober, E. M.; Caspar, J. V.; Sullivan, B. P.; Meyer, T. J. *Inorg. Chem.* **1988**, *27*, 4587−4598.
(28) Dobson, J. C.; Meyer, T. J. *Inorg. Chem.* **1989**, *28*, 2013−2016.
(29) Costentin, C.; Robert, M.; Savé ant1, J. M.; Teillout, A. L. *Proc. Natl. Acad. Sci. U.S.A.* **2009**, *106*, 11829−11836.
(30) Che, C.-M.; Yam, V. W. W.; Cho, K. C.; Gray, H. B. *J. Chem. Soc., Chem. Commun.* **1987**, 948−949.
(31) Schindler, S.; Castner, E. W., Jr.; Creutz, C.; Sutin, N. *Inorg. Chem.* **1993**, *32*, 4200−4208.
(32) Chin, K. F.; Cheng, Y. K.; Cheung, K. K.; Guo, C. X.; Che, C.-M. *J. Chem. Soc., Dalton Trans.* **1995**, 2967−2973.
(33) Cheng, J. Y. K.; Cheung, K. K.; Che, C. M.; Lau, T. C. *Chem. Commun.* **1997**, 1443−1444.
(34) Sugimoto, H.; Kitayama, K.; Ashikari, K.; Matsunami, C.; Ueda, N.; Umakoshi, K.; Hosokoshi, Y.; Sasaki, Y.; Itoh, S. *Inorg. Chem.* **2011**, *50*, 9014−9023.
(35) Burla, M. C.; Caliandro, R.; Camalli, M.; Carrozzini, B.; Cascarano, G. L.; De Caro, L.; Giacovazzo, C.; Polidori, G.; Siliqi, D.; Spagna, R. *SIR2008*; 2007.
(36) *Crystal Structure 3.8: Crystal Structure Analysis Package*; Rigaku Corp.: The Woodlands, TX, 2000−2006.
(37) Frisch, M. J.; et al. *Gaussian 09*, revision C.01; Gaussian, Inc.: Wallingford, CT, 2009.
(38) (a) Lee, C.; Yang, W.; Parr, R. G. *Phys. Rev. B* **1988**, *37*, 785−789. (b) Becke, A. D. *J. Chem. Phys.* **1993**, *98*, 5648−5652.
(39) (a) Pidun, U.; Boehme, C.; Frenking, G. *Angew. Chem., Int. Ed. Engl.* **1996**, *35*, 2817−2820. (b) Dapprich, S.; Ujaque, G.; Maseras, F.; Lledós, A.; Musaev, D. G.; Morokuma, K. *J. Am. Chem. Soc.* **1996**, *118*, 11660−11661. (c) Haller, J.; Strassner, T.; Houk, K. N. *J. Am. Chem. Soc.* **1997**, *119*, 8031−8034. (d) Delmonte, A. J.; Haller, J.; Houk, K. N.; Sharpless, K. B.; Singleton, D. A.; Strassner, T.; Thomas, A. A. *J. Am. Chem. Soc.* **1997**, *119*, 9907−9908.
(40) Nova, A.; Ujaque, G.; Maseras, F.; Lledós, A.; Espinet, P. *J. Am. Chem. Soc.* **2006**, *128*, 14571−14578.
(41) (a) Goossen, L. J.; Koley, D.; Hermann, H. L.; Thiel, W. *J. Am. Chem. Soc.* **2005**, *127*, 11102−11114. (b) Goossen, L. J.; Koley, D.; Hermann, H. L.; Thiel, W. *Organometallics* **2006**, *25*, 54−67. (c) Álvarez, R.; Faza, O. N.; López, C. S.; de Lera, Á. R. *Org. Lett.* **2006**, *8*, 35−38. (d) Hicks, J. D.; Hyde, A. M.; Cuezva, A. M.; Buchwald, S. L. *J. Am. Chem. Soc.* **2009**, *131*, 16720−16734.
(42) Ariafard, A.; Yates, B. F. *J. Am. Chem. Soc.* **2009**, *131*, 13981−13991.
(43) Surawatanawong, P.; Hall, M. B. *Organometallics* **2008**, *27*, 6222−6232.
(44) Lan, Y.; Wang, C.; Sowa, J. R.; Wu, Y.-D. *J. Org. Chem.* **2010**, *75*, 951−954.
(45) Maestri, G.; Motti, E.; Della Ca', N.; Malacria, M.; Derat, E.; Catellani, M. *J. Am. Chem. Soc.* **2011**, *133*, 8574−8585.
(46) Hay, P. J.; Wadt, W. R. *J. Chem. Phys.* **1985**, *82*, 299−310.
(47) (a) Fukui, K. *J. Phys. Chem.* **1970**, *74*, 4161−4163. (b) Fukui, K. *Acc. Chem. Res.* **1981**, *14*, 363−368.
(48) (a) Gonzalez, C.; Schlegel, H. B. *J. Chem. Phys.* **1989**, *90*, 2154−2161. (b) Gonzalez, C.; Schlegel, H. B. *J. Phys. Chem.* **1990**, *94*, 5523−5527.
(49) (a) Hratchian, H. P.; Schlegel, H. B. *J. Chem. Phys.* **2004**, *120*, 9918−9924. (b) Hratchian, H. P.; Schlegel, H. B. *J. Chem. Theory Comput.* **2005**, *1*, 61−69.
(50) Dolg, M.; Wedig, U.; Stoll, H.; Preuss, H. *J. Chem. Phys.* **1987**, *86*, 866−872.
(51) (a) Wachters, A. J. H. *J. Chem. Phys.* **1970**, *52*, 1033−1036. (b) Hay, P. J. *J. Chem. Phys.* **1977**, *66*, 4377−4384. (c) Trucks, G. W.; Raghavachari, K. *J. Chem. Phys.* **1989**, *91*, 1062−1065.
(52) Grimme, S. *J. Comput. Chem.* **2006**, *27*, 1787−1799.
(53) (a) Zhao, Y.; Truhlar, D. G. *Theor. Chem. Acc.* **2008**, *120*, 215−241. (b) Zhao, Y.; Truhlar, D. G. *Acc. Chem. Res.* **2008**, *41*, 157−167.
(54) (a) Takahara, Y.; Fueno, T.; Yamaguchi, K. *Chem. Phys. Lett.* **1989**, *157*, 211−216. (b) Yamaguchi, K.; Okumura, M.; Mori, W.; Maki, J.; Takada, K.; Noro, T.; Tanaka, K. *Chem. Phys. Lett.* **1993**, *210*, 201−210. (c) Kitagawa, Y.; Saito, T.; Ito, M.; Shoji, M.; Koizumi, K.; Yamanaka, S.; Kawakami, T.; Okumura, M.; Yamaguchi, K. *Chem. Phys. Lett.* **2007**, *442*, 445−450.
(55) Reed, A. E.; Weinhold, F. *J. Chem. Phys.* **1985**, *83*, 1736−1740.
(56) (a) Miertuš, S.; Scrocco, E.; Tomasi, J. *Chem. Phys.* **1981**, *5*, 117−129. (b) Tomasi, J.; Mennucci, B.; Cammi, R. *Chem. Rev.* **2005**, *105*, 2999−3093.
(57) Scalmani, G.; Frisch, M. J. *J. Chem. Phys.* **2010**, *132*, 114110.
(58) Chantooni, M. K., Jr.; Kolthoff, I. M. *Anal. Chem.* **1979**, *51*, 133−140.
(59) Sugimoto, H.; Matsunami, C.; Koshi, C.; Yamasaki, M.; Umakoshi, K.; Sasaki, Y. *Bull. Chem. Soc. Jpn.* **2001**, *74*, 2091−2099.
(60) The catalytic dihydroxylation of cyclohexene was carried out in water without acetate buffer, where the yield of diol was 70%. Excellent yields were also obtained at pH 6.0 and 8.0 in the KH_2PO_4−Na_2HPO_4 buffer solutions (Table S2). These results unambiguously indicate that peracetic acid formation was not required in the present catalytic system. The somewhat lower yield (70%) in water as compared to the yield in the buffer solutions may be attributed to unstable pH conditions in water. As clearly shown in Table S2 and Figure 3, pH control is critical in the present catalytic reaction.
(61) No distinctive intermediate such as Os^{III}−OOH was detected in the direct reaction of **2** or **3** with H_2O_2 by UV−vis, resonance Raman, and ESI−MS spectral methods under the experimental conditions employed.

(62) Pourbax, M. *Atlas of Electrochemical Equilibrium in Aqueous Solutions*; NACE: Houston, TX, 1966.
(63) The catalytic 1,2-dihydroxylation of cyclohexene with 29% $H_2{}^{16}O_2$ in a labeled $H_2{}^{18}O$ (H_2O:$H_2{}^{18}O$ = 2:98) gave the diol product containing $C_6H_{12}{}^{16}O_2$, $C_6H_{12}{}^{16}O^{18}O$, and $C_6H_{12}{}^{18}O_2$ in a 15:53:32 ratio. The result clearly demonstrates that the alkene oxidation competed with label exchange of the oxygen atoms in $Os^{V}(O)(OH)$ unit with the oxygen atom of water.
(64) Nelson, D. W.; Gypser, A.; Ho, P. T.; Kolb, H. C.; Kondo, T.; Kwong, H.-L.; McGrath, D. V.; Rubin, A. E.; Norrby, P.-O.; Gable, K. P.; Sharpless, K. B. *J. Am. Chem. Soc.* **1997**, *119*, 1840−1858.
(65) Yip, W.-P.; Yu, W.-Y.; Zhu, N.; Che, C.-M. *J. Am. Chem. Soc.* **2005**, *127*, 14239−14249.
(66) Chen, K.; Costas, M.; Kim, J.; Tipton, A. K.; Que, L., Jr. *J. Am. Chem. Soc.* **2002**, *124*, 3026−3035.
(67) Prat, I.; Mathieson, J. S.; Güell, M.; Ribas, X.; Luis, J. M.; Cronin, L.; Costas, M. *Nat. Chem.* **2011**, *3*, 788−793.
(68) The stepwise pathway cannot be found in this reaction by geometry optimization.